Numerical Conformal Bootstrap

Author: Zhengchen Song
Student number: K21214283

Supervisor: Dr. Petr Kravchuk
Module Code: 7CCMTP50

09/07/2023

Abstract

n-point correlation functions calculate the expectation values of a set of operators in the time order. In Quantum Field Theory, it can be used to compute the probability of fields scattering in terms of the S-matrix. While in Ising models, it can be interpreted as path integrals. The connection between Ising models and field theories gives rise to the phase transition description [1].

There are two ways to study n-point correlation functions, one is the perturbation theory e.g. Feynman diagrams, and the other one is non-perturbative procedures e.g. the confromal bootstrap. In Conformal Field Theory (CFT), the conformal symmetry will allow us to fix the form of n-point functions with a small set of information called CFT data. By using the CFT data only, one can derive the crossing equation. The conformal bootstrap uses the crossing to find some interesting features about the sacling dimension. Also, the conformal bootstrap has been used to find solutions for Ising models in [2, 3].

In Ising lattice models, the correlation length is infinity at the critical point, where the scale invariance has been found. At the critical point, the Ising lattice models can formulate the Ising CFT model, which describes the long distance behavior with an enhanced conformal symmetry [4, 5]. The 2D Ising CFT model was solved analytically in [6, 7], but Ising models of higher odd dimensions remains unsolved. However, a numerical technique has been developed to solve 3D Ising models in [2, 3], and $O(N)$ vector models in [8].

In this dissertation, We will use numerical bootstrap to study the scaling dimensions of the operators in a correlation function with respect to the scaling dimensions of other operators, which we will discuss in Chapter 4. To build the layout for the conformal bootstrap, we start with basic knowledge of QFT, and then introduce the radial quantization in Chapter 1. In Chapter 2, we will show that the OPE is naturally gifted once the radial quantization is settled. One last step before the conformal bootstrap is Chapter 3, in which we will use the crossing symmetry to study the 4-point functions, giving the crossing equation which is related to the functional in the conformal bootstrap.

After finishing the set-up for the conformal bootstrap, we will give an interesting example on how the conformal bootstrap solves the crossing equation. Then we use the numerical bootstrap to study the 2D Ising model and 3D Ising model in details, and we find the convergent behavior for the numerical solution when we further improve the values of various approximation parameters involved.

Contents

1 Quantum Field Theory and Conformal Symmetry

In Quantum Field Theory (QFT), a n-point correlation function of scalar operators[1] has the form [9],

$$\langle\phi_1(x_1)\phi_2(x_2)...\phi_n(x_n)\rangle \equiv \langle 0|T\{\phi_1(x_1)\phi_2(x_2)...\phi_n(x_n)\}|0\rangle \ , \tag{1.1}$$

where each ϕ_i is a scalar operator with position x_i in time ordered. In Conformal Field Theory (CFT), the correlator has the property,

$$\langle\phi_1(x_1')\phi_2(x_2')...\phi_n(x_n')\rangle = \Omega^{\Delta_1}(x_1)\Omega^{\Delta_2}(x_2)...\Omega^{\Delta_n}(x_n)\,\langle\phi_1(x_1)\phi_2(x_2)...\phi_n(x_n)\rangle \ , \tag{1.2}$$

where primed coordinate on the L.H.S. means operators after conformal transformations,

$$U\phi(x)U^{-1} = \Omega^{\Delta}(x')\phi'(x') \ , \tag{1.3}$$

where U is the conformal transformation generated by the conformal algebras. In the QFT case, $\Omega^{\Delta}(x') = 1$.

The rescaling Ω^{Δ} is characterized by a scaling dimension Δ,

$$D\ \mathcal{O}(0)\,|0\rangle = \Delta\ \mathcal{O}(0)\,|0\rangle \ , \quad K^{\mu}\ \mathcal{O}(0)\,|0\rangle = 0 \tag{1.4}$$

where D and K^{μ} are conformal generators, and $\mathcal{O}(0)$ is called the primary operator. In the following subsections, we will first introduce the conformal generators, and explain primary operators in the context of radial quantization, which leads to the state-operator correspondence. In the last subsection, we will discuss the unitarity bounds using both conformal algebras and state-operator corresponds.

1.1 Conformal Algebras

As an extension to the generators of Poincaré group, the commutation relations of conformal generators are [10],

$$\begin{aligned}
[M_{\mu\nu}, P_\rho] &= \delta_{\nu\rho}P_\mu - \delta_{\mu\rho}P_\nu \\
[M_{\mu\nu}, K_\rho] &= \delta_{\nu\rho}K_\mu - \delta_{\mu\rho}K_\nu \\
[M_{\mu\nu}, M_{\rho\sigma}] &= \delta_{\nu\rho}M_{\mu\sigma} - \delta_{\mu\rho}M_{\nu\sigma} + \delta_{\nu\sigma}M_{\rho\mu} - \delta_{\mu\sigma}M_{\rho\nu} \\
[D, P_\mu] &= P_\mu \\
[D, K_\mu] &= -K_\mu \\
[K_\mu, P_\nu] &= 2\delta_{\mu\nu}D - 2M_{\mu\nu} \ ,
\end{aligned} \tag{1.5}$$

where $M_{\mu\nu}$ are the generators of the $\mathfrak{so}(d)$ Lie algebra up to an isomorphism in the Euclidean signature, and P_μ is the translation generator. In additional to already known Poincaré generators, there are $d+1$ extra generators brought by the conformal symmetry, which give the definition of scaling dimension and primary operators in (1.4). They are the dilatation operator D, and

[1] The operator with spins can be difficult, here we only introduce the definition with scalars.

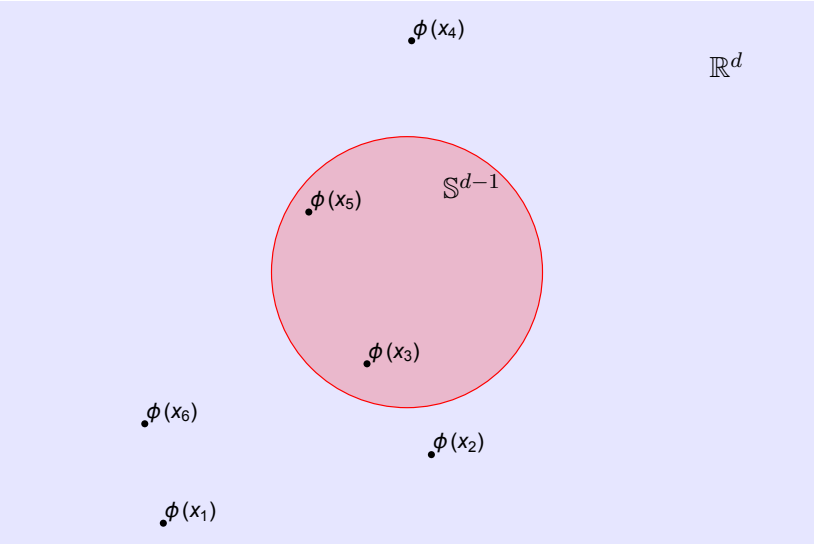

Figure 1: This is the configuration of the radial quantization in $\mathbb{R}^d$. The red disk is the interior region, and the red sphere denotes the boundary between interior and exterior. There are six points spilt on the $\mathbb{R}^d$, divided by the boundary. In this case, the path integral over the interior including $\phi(x_3)$ and $\phi(x_5)$ gives the states on the sphere.

the special conformal transformation operator K_μ. Before using state-operator correspondence, let us define primary operators (or primaries) in terms of algebras,

$$[K_\mu, \mathcal{O}(0)] = 0 \ , \quad [D, \mathcal{O}(0)] = \Delta \mathcal{O}(0) \ , \tag{1.6}$$

where $\mathcal{O}(0)$ is the primary.

1.2 Radial Quantization

A correlation function can be computed by using path integral [9],

$$\langle \phi(x_1)...\phi(x_n) \rangle = \frac{1}{\mathcal{N}} \int \mathcal{D}\phi \ \phi(x_1)...\phi(x_n) e^{-S} \ , \tag{1.7}$$

where $\mathcal{N} = \int \mathcal{D}\phi \ e^{-S}$ is the normalization factor. In radial quantization, we can split the integration variable $\mathcal{D}\phi$ into three parts, the interior, the exterior, and the boundary of a ball (See Fig. 1). So the integral becomes,

$$\int \mathcal{D}\phi \ \phi(x_1)...\phi(x_n) e^{-S} = \int \mathcal{D}\phi_{\rm b} \int \mathcal{D}\phi_{\rm in} \prod_{x_k \in \text{interior}} \phi(x_k) e^{-S} \int \mathcal{D}\phi_{\rm ex} \prod_{x_l \in \text{exterior}} \phi(x_l) e^{-S} \ , \tag{1.8}$$

where we separate points inside and outside the boundary then have a product of three terms. Since we want a continous integral, the scalars inside and outside should agree on the boundary. So the value of a path integral over the interior or the exterior is defined by the states on the

boundary,

$$\int \mathcal{D}\phi_{\rm b} \int \mathcal{D}\phi_{\rm in} \prod_{x_k\in\text{interior}} \phi(x_k)e^{-S} \int \mathcal{D}\phi_{\rm ex} \prod_{x_l\in\text{exterior}} \phi(x_l)e^{-S} = \int \mathcal{D}\phi_{\rm b}\Psi_{\rm in}(\phi_b)\Psi_{\rm ex}(\phi_b) \ ,$$
$$\int \mathcal{D}\phi_{\rm b}\Psi_{\rm in}(\phi_b) \equiv \int \mathcal{D}\phi_{\rm in} \prod_{x_k\in\text{interior}} \phi(x_k)e^{-S} \ , \tag{1.9}$$
$$\int \mathcal{D}\phi_{\rm b}\Psi_{\rm ex}(\phi_b) \equiv \int \mathcal{D}\phi_{\rm ex} \prod_{x_l\in\text{exterior}} \phi(x_l)e^{-S} \ ,$$

which means a path integral over some region gives a boundary state $\Psi_{\rm in/ex}(\phi_b)$.

1.3 State-Operator Correspondence

Our states $|\Psi\rangle$ now are prepared by doing path integrals over some region with some operators insertion, and the vaccum is given by path integrals with no operator insertion. So the Hilbert is spanned by the boundary states $|\phi_b\rangle$ [10],

$$|\Psi\rangle = \int \mathcal{D}\phi_b \ \langle\phi_b|\Psi\rangle \, |\phi_b\rangle \ . \tag{1.10}$$

Let's first see how the vaccum is expanded in this way,

$$\begin{aligned} |0\rangle &= \int \mathcal{D}\phi_b \ \langle\phi_b|0\rangle \, |\phi_b\rangle \\ &= \int \mathcal{D}\phi_b \ |\phi_b\rangle \int_{\phi(x)|_{\text{boundary}}=\phi_b} \mathcal{D}\phi(x) \ e^{-S[\phi(x)]} \ , \end{aligned} \tag{1.11}$$

where $\phi(x) = 0$ outside the boundary. The second line of (1.11) is the path integral with no operators inserted in the interior. We can insert a operator in the interior to create the corresponding state in terms of the basis ϕ_b,

$$\mathcal{O}(y)\,|0\rangle = \int \mathcal{D}\phi_b \ |\phi_b\rangle \int_{\phi(x)|_{\text{boundary}}=\phi_b} \mathcal{D}\phi(x) \ \mathcal{O}(y)e^{-S[\phi(x)]} \ , \tag{1.12}$$

where y can be any points in $\mathbb{R}^d$, as long as it is inside the boundary. If $y = 0$, we denote $\mathcal{O}(0)\,|0\rangle \equiv |\mathcal{O}\rangle$.

The relation above brings an operator to a state. We can also do it reversely. Suppose we have a state $|O_i\rangle$ in the Hilbert space, we can find the corresponding $\mathcal{O}(0)$ operator inserted at the origin of some sphere, and the sphere is in $\mathbb{R}^d$ with its origin at x_i. There is a one-one correspondence between states and operators,

$$\mathcal{O}(0) \ \longleftrightarrow \ \mathcal{O}(0)\,|0\rangle \equiv |\mathcal{O}\rangle \ . \tag{1.13}$$

The relation above is called the state-operator correspondence. Together with the conformal algebras (1.5), we find the following correspondence,

$$\begin{aligned} [K_\mu, \mathcal{O}(0)] = 0 \quad &\longleftrightarrow \quad K_\mu|\mathcal{O}\rangle = 0 \ , \\ [D, \mathcal{O}(0)] = \Delta\mathcal{O}(0) \quad &\longleftrightarrow \quad D|\mathcal{O}\rangle = \Delta|\mathcal{O}\rangle \ , \\ [M_{\mu\nu}, \mathcal{O}(0)] = \mathcal{S}_{\mu\nu}\mathcal{O}(0) \quad &\longleftrightarrow \quad M_{\mu\nu}|\mathcal{O}\rangle = \mathcal{S}_{\mu\nu}|\mathcal{O}\rangle \ . \end{aligned} \tag{1.14}$$

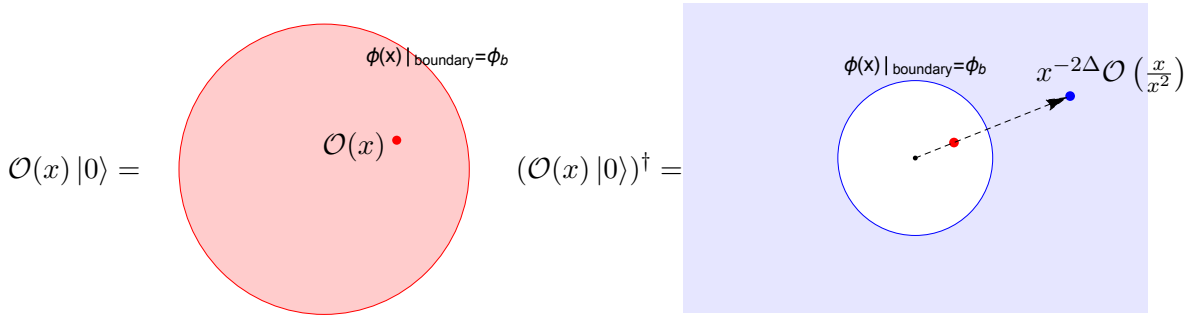

Figure 2: A state can be made by taking the path integral over some region that includes operator. And the dual state is made by inserting the operator at the point which is inverse to the origin (1.15), and then perform the path integral over the exterior.

To build the complete theory of radial quantization, we still need to define ket vectors. We start with defining the Hermitian conjugate of operators,

$$\mathcal{O}(x)^\dagger = x^{-2\Delta}\mathcal{O}\left(\frac{x}{x^2}\right) \ , \tag{1.15}$$

so the ket vectors are given by state-operator correspondence,

$$(\mathcal{O}(x)\,|0\rangle)^\dagger = \langle 0|\, x^{-2\Delta}\mathcal{O}\left(\frac{x}{x^2}\right) \ . \tag{1.16}$$

The Hermitian conjugates of conformal algebras are,

$$\begin{aligned} M_{\mu\nu}^\dagger &= -M_{\mu\nu} \ , \\ D^\dagger &= D \ , \\ P_\mu^\dagger &= K_\mu \ . \end{aligned} \tag{1.17}$$

We use exponential map e^{iX} to generate a conformal transformation operator U as in 1.2, then we can act it on an operator in the form of $e^{iX}\mathcal{O}e^{-iX}$. The transformation is called unitary transformation if e^{iX} is unitary, i.e. X is Hermitian. One can build a Hermitian basis from (1.17),

$$\begin{aligned} (iM_{\mu\nu})^\dagger &= iM_{\mu\nu} \ , \\ D^\dagger &= D \ , \\ (P_\mu + K_\mu)^\dagger &= P_\mu + K_\mu \ , \\ [i(P_\mu - K_\mu)]^\dagger &= i(P_\mu - K_\mu) \ , \end{aligned} \tag{1.18}$$

the basis above will span a $\mathfrak{so}(2,d)$ algebra.

1.4 Unitarity Bounds

The unitary transformation preserves the norm, that's why we want Hermitian operators in QFT. So we can changed our basis of the conformal algebras (1.5) into a Hermitian basis in the Euclidean CFT, we have $\mathfrak{so}(2,d)$ algebra (1.18) as the time direction has the same sign as spatial directions. Recall that the Euclidean theory is the Lorentzian theory after a Wick rotation,

$$\mathcal{O}_E(t_E,\vec{x}) \equiv \mathcal{O}_L(-it_E,\vec{x}) = e^{iH(-it_E)-i\vec{x}\cdot\vec{P_L}}\mathcal{O}_L(0,0)e^{-iH(-it_E)+i\vec{x}\cdot\vec{P_L}} \ , \tag{1.19}$$

then take Hermitian conjugates of both sides,

$$\mathcal{O}_E(t_E,\vec{x})^\dagger = \mathcal{O}_E(-t_E,\vec{x}) \ . \tag{1.20}$$

The norms of states in Lorentzian signature should be non-negative,

$$\langle \mathcal{O}_L|\mathcal{O}_L\rangle = \langle 0|\, \mathcal{O}_L(-it_E,\vec{x})^\dagger \mathcal{O}_L(-it_E,\vec{x})\,|0\rangle = \langle 0|\, \mathcal{O}_E(-t_E,\vec{x})\mathcal{O}_E(t_E,\vec{x})\,|0\rangle \geq 0 \ , \tag{1.21}$$

the positivity constraint above is called the reflection positivity. The state-operator correspondence tells us that (1.21) is equivalent to a path integral over a region with operators inserted in reflected time directions having a positive value.

We followed the notes [10] to find the unitarity bound. The norm of primary operators ($\mathcal{O}^\mu$) are automatically positive semi-definite due to the normalization,

$$\langle \mathcal{O}_\mu|\mathcal{O}^\nu\rangle = \delta_\mu^{\ \nu} \ , \tag{1.22}$$

where μ and ν are indices for representations of $SO(d)$.

The unitarity bound is obtained by looking at the norm of their descendants. All descendants are parts of the Hilbert space, so the norm of which should be non-negative as well,

$$\begin{aligned} \langle \mathcal{O}_\mu|(P^a)^\dagger P^b|\mathcal{O}^\nu\rangle &= \langle \mathcal{O}_\mu|K^a P^b|\mathcal{O}^\nu\rangle \\ &= \langle \mathcal{O}_\mu|[K^a,P^b]|\mathcal{O}^\nu\rangle \\ &= \langle \mathcal{O}_\mu|2D\delta_{ab} - 2M_{ab}|\mathcal{O}^\nu\rangle \end{aligned} \tag{1.23}$$

where (1.17) is used in the first step, and (1.5) in the last step. One naive approach is to look at the diagonal components of (1.23), and apply the positive semi-definite condition,

$$\mathrm{Tr}\left[\langle \mathcal{O}_\mu|2D\delta_{ab} - 2M_{ab}|\mathcal{O}^\nu\rangle\right] \propto \Delta \geq 0 \ , \tag{1.24}$$

where the trace suppresses the anti-symmetric term M_{ab}, and leaves D alone. The eigenvalue of D is given according to (1.14) as the last step.

On the other hand, the off-diagonal structure of (1.23) reveals a stronger unitarity bound,

$$\langle \mathcal{O}_\mu|2D\delta_{ab} - 2M_{ab}|\mathcal{O}^\nu\rangle = 2\Delta(\delta_{ab})_\mu^{\ \nu} - 2(S_{ab})_\mu^{\ \nu} \geq 0, \tag{1.25}$$

where S_{ab} is the eigenvalue of M_{ab} according to (1.14). Next we take determinants of both sides,

$$\mathrm{Det}[\Delta(\delta_{ab})_\mu^{\ \nu} - (S_{ab})_\mu^{\ \nu}] \geq 0 \ , \tag{1.26}$$

where $(\delta_{ab})_\mu^{\ \nu}$ is the identity, and the equation is saturated when Δ is the eigenvalue of $(S_{ab})_\mu^{\ \nu}$, i.e.

$$\Delta \geq \mathrm{Max}[\lambda_n] \ , \tag{1.27}$$

where λ_n are all possible eigenvalues of $(S_{ab})_\mu^{\ \nu}$. Any anti-symmetric matrix can be written as,

$$(S_{ab})_\mu^{\ \nu} = (S_{[ab]})_\mu^{\ \nu} = (I^{\alpha\beta})_{[ab]}(S_{\alpha\beta})_\mu^{\ \nu} \ , \tag{1.28}$$

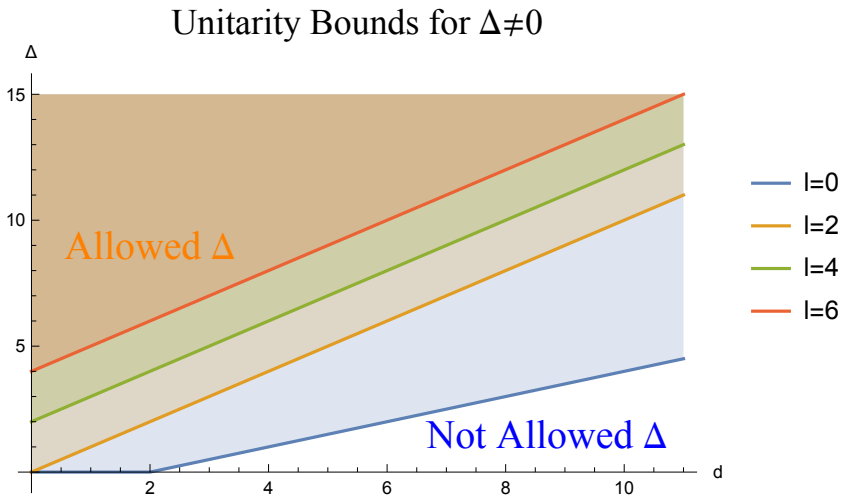

Figure 3: The horizontal axis is the spacetime dimension d, and the vertical axis is the scaling dimension Δ. l is the rank of a traceless symmetric irreducible representation V_l over $\mathrm{R}_{\mathcal{O}}$. For $\Delta \neq 0$ cases, regions above the lines denote allowed scaling dimensions Δ with respect to different l, i.e. satisfying the unitarity bounds.

where $(I^{\alpha\beta})_{[ab]} \equiv \delta^{\alpha}_{\ [a}\delta^{\beta}_{\ b]}$. Ignoring the indices (a, b, μ, ν) in (1.28) can we write,

$$I \cdot S = \left((I+S)^2 - I^2 - S^2\right)/2 \ , \tag{1.29}$$

where all quaratic terms are Casimir operators. Recall that I is the generator under vector representation V_1, S the generator under some other irreducible representation $\mathrm{R}_{\mathcal{O}}$, and $I+S$ the generator under $V_1 \otimes \mathrm{R}_{\mathcal{O}}$. They are representations of $SO(d)$. To get the maximum eigenvalue of $I \cdot S$, one needs to find the maximum of $(I+S)^2$ after deciding the S, i.e. the $\mathrm{R}_{\mathcal{O}}$. Making the choice of $\mathrm{R}_{\mathcal{O}} = V_l$, where l denotes the spin-l traceless symmetric tensor representation, and writing (1.29) in terms of Casimir operators,

$$\begin{aligned} I \cdot S &= \left(-\mathrm{Cas}[V_{l-1}] + \mathrm{Cas}[V_1] + \mathrm{Cas}[V_l]\right)/2 \\ \mathrm{Cas}[V_l] &= l(l+d-2) \ , \end{aligned} \tag{1.30}$$

where the Casimir operator of V_{l-1} is the minimum among all irreducible representations, and the direct sum of which is $V_1 \oplus V_l$. Recall that Δ should be greater than any of these Casimirs (1.27), so the stronger unitarity bound is,

$$\Delta \geq l + d - 2 \ . \tag{1.31}$$

But now the problem is obvious, if $l = 0$, the first term in (1.30) becomes $\mathrm{Cas}[V_{-1}]$. Negative dimension is non-physical, so we need to find another unitarity bound for $l = 0$ special case. The unitarity bound including $l = 0$ is revealed in the second derivative of primaries,

$$\begin{aligned} \langle \mathcal{O}_\mu | K^a K_a P^b P_b | \mathcal{O}^\nu \rangle &= \langle \mathcal{O}_\mu | [K^a, P^b][K_a, P_b] + K^a [K_a, P^b] P_b | \mathcal{O}^\nu \rangle \\ &= \langle \mathcal{O}_\mu | \, 4dD^2 - 4M^2 + 2(D+1)(2\delta^a_{\ a} D - 2M^a_{\ a}) \\ &\qquad - 2(d-1)(2\delta^a_{\ a} D - 2M^a_{\ a}) - 2M_a^{\ b}(2\delta^a_{\ b} D - 2M^a_{\ b}) \, | \mathcal{O}^\nu \rangle \\ &= \langle \mathcal{O}_\mu | 4dD^2 + 2(D+1)(2dD) - 2(d-1)(2dD) | \mathcal{O}^\nu \rangle \\ &= \delta_\mu^{\ \nu}(2\Delta + 2 - d)(4d\Delta) \ , \end{aligned} \tag{1.32}$$

this unitarity bound includes $l = 0$, but the price to pay is being less stronger than (1.31),

$$\Delta = 0 \ , \ \text{or} \quad \Delta \geq \frac{d-2}{2} \ . \tag{1.33}$$

To conclude, merging both unitarity bounds (1.31, 1.33) gives,

$$\begin{cases} \Delta = 0 \ , \ \text{or} \\ \Delta \geq \begin{cases} \dfrac{d-2}{2} & l = 0 \\ l + d - 2 & l > 0 \ . \end{cases} \end{cases} \tag{1.34}$$

Fig. 3 shows how Δ is constrained by the unitarity bounds, the interception of the y-axis is the minimum allowed Δ. One can also shift the y-axis to the corresponding the d to get minimum allowed Δ with respect to spacetime dimension. In Chapter 4, we will see that the minimum allowed Δ is very important for the conformal bootstrap.

2 Operator Product Expansion

A state can be expanded into an infinite sum over primaries and descendants,

$$\mathcal{O}(x)|0\rangle = e^{x\cdot P}\mathcal{O}(0)e^{-x\cdot P}|0\rangle = e^{x\cdot P}|\mathcal{O}\rangle = \sum_{n=0}^{\infty}\frac{1}{n!}(x\cdot P)^n|\mathcal{O}\rangle \ , \tag{2.1}$$

where P^μ is the translation generator in (1.5). Given two operators inserted in $\mathbb{R}^d$, we have the corresponding state by performing the path integral over a sphere, in which both operators are included, using (2.1) we have [11],

$$\mathcal{O}_1(x)\mathcal{O}_2(0)\,|0\rangle = \sum_k C_{12k}(x,P)\mathcal{O}_k(0)\,|0\rangle \ , \tag{2.2}$$

where $C_{12k}(x,P)$ are some coefficients fixed by the conformal symmetry up to an overall factor. The coefficient C_{12k} contains operator P, which gives descendants when acting on primaries $\mathcal{O}_k$, so the R.H.S of (2.2) can cover all kinds of operators (as in (2.1)). Recall that using state-operator correspondence, a path integral gives a state in the Hilbert space. We can also performed the path integral around some other origin, the choice is arbitrary. The Operator Product Expansion (OPE) is,

$$\mathcal{O}_1(x_1)\mathcal{O}_2(x_2)\,|0\rangle = \sum_k C_{12k}(x_{13},x_{23},\partial_{x_3})\mathcal{O}_k(x_3)\,|0\rangle \ , \tag{2.3}$$

where x_3 is an arbitrary point in $\mathbb{R}^d$. The configuration of (2.2,2.3) in terms of path integral is shown in Fig. 4.

We give the definition of OPE for operators with spins without proof [10],

$$\mathcal{O}_1^\alpha(x_1)\mathcal{O}_2^\beta(x_2)\,|0\rangle = \sum_{k,\gamma} C_{12k}^{\alpha\beta\gamma}(x_{13},x_{23},\partial_{x_3})\mathcal{O}_k^\gamma(x_3)\,|0\rangle \ , \tag{2.4}$$

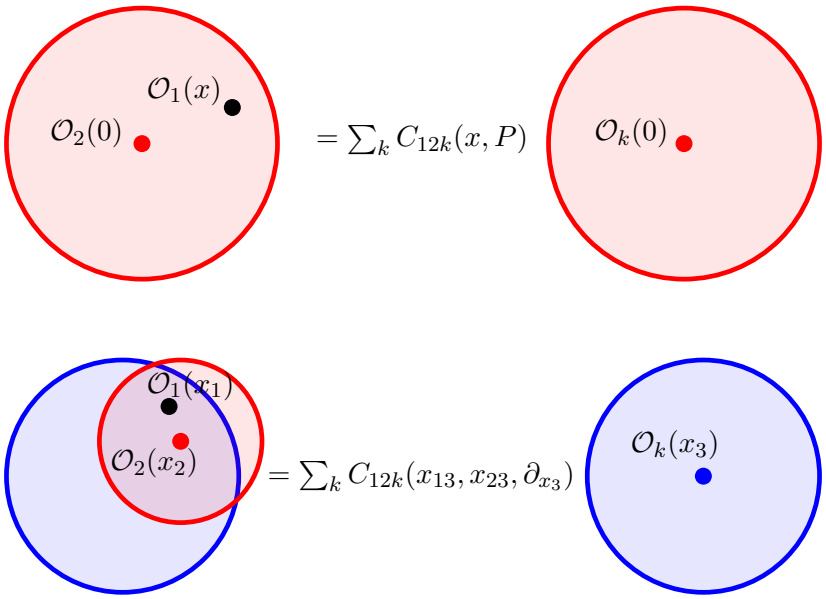

Figure 4: The path integral of two operators insertion is equal to a sum over the path integral of one operator insertion with some coefficients C_{12k}.

where (α, β, γ) are indices for $SO(d)$ representation. For example, under V_l traceless symmetric tensor representation $\mathcal{O}^\alpha \equiv \mathcal{O}^{\mu_1 \cdots \mu_l}$, where μ_l are tensor indices. We can use the orthonormal basis for primary operators s.t. the 2-point function is [12],

$$\langle \mathcal{O}_i^\alpha(x) \mathcal{O}_j^\beta(0) \rangle = \delta_{ij} \frac{I^{\alpha\beta}(x)}{x^{\Delta_i + \Delta_j}} \ , \tag{2.5}$$

where $I^{\alpha\beta}(x) = I^{(\mu_1\nu_1}(x) ... I^{\mu_l\nu_l)}(x)$, and $I^{\mu\nu}(x)$ is defined as,

$$I^{\mu\nu}(x) = \delta^{\mu\nu} - 2\frac{x^\mu x^\nu}{x^2} \ . \tag{2.6}$$

3 Conformal Blocks

3.1 4-point Function

Thanks to the scale invariance property (1.2), 2-point functions after normalization are fixed up to a scaling dimension [4],

$$\langle \phi(x)\phi(y) \rangle = |x - y|^{-2\Delta_\phi} \ , \tag{3.1}$$

where Δ_ϕ is the scaling dimension. We can see that the 2-point function only depends on the distance between x and y. The operators should not be constrained to this particular kind of scalar(In fact, operators with any spins are allowed), so the generic form of arbitrary scalar operators is,

$$\langle \mathcal{O}_i(x)\mathcal{O}_j(y) \rangle = \delta_{ij} |x - y|^{-(\Delta_i + \Delta_j)} \ , \tag{3.2}$$

Recall that we have OPE for all n-point function, which can reduce the number of points by one for each time performed. Therefore, all n-point functions are fixed by 2-point functions of

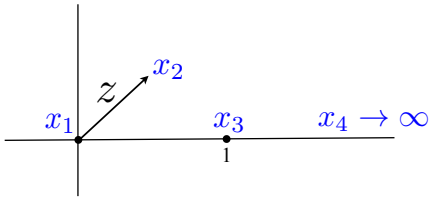

Figure 5: Figure from [13]

any pairs from n points. The simplest example is the 3-point function,

$$\langle \mathcal{O}_1(x_1)\mathcal{O}_2(x_2)\mathcal{O}_3(x_3)\rangle = f_{123}|x_{12}|^{-\Delta_{12}}|x_{23}|^{-\Delta_{23}}|x_{31}|^{-\Delta_{31}} \ , \tag{3.3}$$

where $|x_{ij}| = |x_1 - x_2|$, and $\Delta_{ij} = \Delta_i + \Delta_j - \Delta_k$. The constant f_{ijk} comes from the OPE coefficient in (2.3). The property of being fixed by 2-point functions can be seen in 4-point functions as well,

$$\langle \mathcal{O}_1(x_1)\mathcal{O}_2(x_2)\mathcal{O}_3(x_3)\mathcal{O}_4(x_4)\rangle = g(u,v)\frac{1}{(x_{12}^2)^{\frac{\Delta_1+\Delta_2}{2}}(x_{34}^2)^{\frac{\Delta_3+\Delta_4}{2}}}\left(\frac{x_{24}^2}{x_{14}^2}\right)^{\frac{\Delta_{12}}{2}}\left(\frac{x_{14}^2}{x_{13}^2}\right)^{\frac{\Delta_{34}}{2}} \ , \tag{3.4}$$

where u and v are also fixed by 2-point functions,

$$u = \frac{x_{12}^2 x_{34}^2}{x_{13}^2 x_{24}^2}, \quad v = \frac{x_{23}^2 x_{14}^2}{x_{13}^2 x_{24}^2} \ , \tag{3.5}$$

To understand what $g(u,v)$ is, we focus on the simplest case of 4-point functions, i.e. four identical scalars $\phi(x)$. We can arrange four points in a plane by using conformal transformations [13], and use Cartesian coordinates to label them. We moved x_1 to the origin $(0,0,...)$, x_2 to $(x,y,...)$, x_3 to $(1,0,...)$, and x_4 to infinity. After doing these transformations, we will use out all the degrees of freedom given by conformal symmetries except for those characterized by u and v, which is defined in (3.5). Therefore, a four identical scalars correlation function is [14],

$$\langle \phi(x_1)\phi(x_2)\phi(x_3)\phi(x_4)\rangle = \frac{g(u,v)}{|x_{12}|^{2\Delta_\phi}|x_{34}|^{2\Delta_\phi}} \ . \tag{3.6}$$

There is a symmetry of swapping any pairs of coordinates for the L.H.S of (3.6), so $g(u,v)$ must obey the following rules unders these procedures,

$$\begin{aligned} &g(u,v) \to g(u/v, 1/v), \quad \text{for } x_1 \leftrightarrow x_2 \text{ or } x_3 \leftrightarrow x_4 \ , \\ &g(u,v) \to \left(\frac{u}{v}\right)^{\Delta_\phi} g(v,u) \quad \text{for } x_1 \leftrightarrow x_3, \text{ or } x_2 \leftrightarrow x_4 \ . \end{aligned} \tag{3.7}$$

Another very useful coordinate in the conformal bootstrap is $(z,\bar{z})$,

$$u = z\bar{z}, \ v = (1-z)(1-\bar{z}), \tag{3.8}$$

and swapping $u \leftrightarrow v$ corresponds to $z \to (1-z)$ and $\bar{z} \to (1-\bar{z})$.

3.2 Conformal Blocks

We still begin with the correlation function in (3.6), but we split the OPE coefficient into two parts[2],

$$\phi(x_1)\phi(x_2) = \sum_{\mathcal{O}} f_{\phi\phi\mathcal{O}} C_\alpha(x_{12}, \partial_{x_2}) \mathcal{O}^\alpha(x_2) \ , \tag{3.9}$$

where Einstein summation is used for α. $f_{\phi\phi\mathcal{O}}$ is the overall factor called the CFT data, and we have another coefficient $C_\alpha(x_{12}, \partial_{x_2})$ completely fixed by the conformal symmetry.

We can do OPE to $\phi(x_1)\phi(x_2)$ and $\phi(x_3)\phi(x_4)$ separately,

$$\begin{aligned} \langle \phi(x_1)\phi(x_2)\phi(x_3)\phi(x_4)\rangle &= \sum_{\mathcal{O},\mathcal{O}'} f_{\phi\phi\mathcal{O}} C_\alpha(x_{12}, \partial_{x_2}) f_{\phi\phi\mathcal{O}'} C_\beta(x_{34}, \partial_{x_4}) \langle \mathcal{O}^\alpha(x_2) \mathcal{O}'^\beta(x_4)\rangle \\ &= \sum_{\mathcal{O}} f^2_{\phi\phi\mathcal{O}} C_\alpha(x_{12}, \partial_{x_2}) C_\beta(x_{34}, \partial_{x_4}) \frac{I^{\alpha\beta}}{x_{24}^{2\Delta_\mathcal{O}}} \ , \end{aligned} \tag{3.10}$$

where (2.5) is used to cancel out one of the summation in the second step. Recall that the 4-point function is fixed by $g(u, v)$, we find the conformal blocks decomposition after comparing (3.6) and (3.10),

$$\begin{aligned} g(u, v) &= \sum_{\mathcal{O}} f^2_{\phi\phi\mathcal{O}} g_{\Delta_\mathcal{O}, l_\mathcal{O}}(u, v) \\ g_{\Delta_\mathcal{O}, l_\mathcal{O}}(u, v) &= x_{12}^{\Delta_\phi} x_{34}^{\Delta_\phi} C_\alpha(x_{12}, \partial_{x_2}) C_\beta(x_{34}, \partial_{x_4}) \frac{I^{\alpha\beta}}{x_{24}^{2\Delta_\mathcal{O}}} \ , \end{aligned} \tag{3.11}$$

where $l_\mathcal{O}$ is the spin of the representation of $SO(d)$. The conformal blocks in 2D is solved in [15],

$$\begin{aligned} g_{\Delta,l}(u, v) &= k_{\Delta+l}(z) k_{\Delta-l}(\bar{z}) + k_{\Delta-l}(z) k_{\Delta+l}(\bar{z}) \\ k_\beta(z) &\equiv z_2^{\beta/2} {}_2F_1(\beta/2, \beta/2, \beta, z) \ , \end{aligned} \tag{3.12}$$

where the relation between (u, v) and $(z, \bar{z})$ is given in (3.8).

4 Conformal Bootstrap

For a 4-point function (3.6) , there is a symmetry under swapping $x_1 \leftrightarrow x_3$, or $x_2 \leftrightarrow x_4$, and the changes on $g(u, v)$ is given by (3.7). So we can have the equation of 4-point functions before and after swapping,

$$\frac{g(u, v)}{|x_{12}|^{2\Delta_\phi} |x_{34}|^{2\Delta_\phi}} = \left(\frac{u}{v}\right)^{\Delta_\phi} \frac{g(v, u)}{|x_{13}|^{2\Delta_\phi} |x_{24}|^{2\Delta_\phi}}$$

$$\sum_{\mathcal{O}} f^2_{\phi\phi\mathcal{O}} g_{\Delta_\mathcal{O}, l_\mathcal{O}}(u, v) = \left(\frac{u}{v}\right)^{\Delta_\phi} \sum_{\mathcal{O}} f^2_{\phi\phi\mathcal{O}} g_{\Delta_\mathcal{O}, l_\mathcal{O}}(v, u) \tag{4.1}$$

$$\sum_{\mathcal{O}} f^2_{\phi\phi\mathcal{O}} (v^{\Delta_\phi} g_{\Delta_\mathcal{O}, l_\mathcal{O}}(u, v) - u^{\Delta_\phi} g_{\Delta_\mathcal{O}, l_\mathcal{O}}(v, u)) = 0 \ .$$

[2] Instead of summing over k like in (2.4), here we use $\mathcal{O}$ itself to indicate different operators.

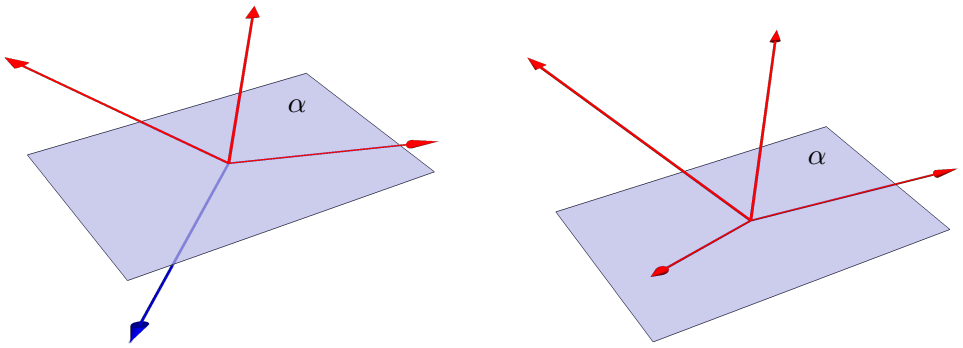

Figure 6: For a non-trivial case, a set of $\vec{F}^{\Delta_\phi}_{\Delta,l}$ that solves the crossing equation (4.1) must satisfy the following statement. For any planes in the space: 1. There are vectors on both sides. 2. There are at least three linear independent vectors on one of the sides (because the dimension of the vector space is three).

We can constrain $f_{\phi\phi\mathcal{O}}$ in a real basis, so $f^2_{\phi\phi\mathcal{O}} \geq 0$. Viewing the term inside the parentheses as an element of the vector space spanned by functions of u and v, we can rewrite (4.1) without any losts of generality,

$$\begin{aligned} \sum_{\Delta,l} p_{\Delta,l} \vec{F}^{\Delta_\phi}_{\Delta,l} &= 0 \\ p_{\Delta,l} &\equiv f^2_{\phi\phi\mathcal{O}} \\ \vec{F}^{\Delta_\phi}_{\Delta,l} &\equiv v^{\Delta_\phi} g_{\Delta_\mathcal{O},l_\mathcal{O}}(u,v) - u^{\Delta_\phi} g_{\Delta_\mathcal{O},l_\mathcal{O}}(v,u) \ . \end{aligned} \tag{4.2}$$

The idea of the crossing equation (4.1) is that there exists a set of positive coefficients $p_{\Delta,l}$ s.t. the sum over vectors with respect to $p_{\Delta,l}$ is zero. Fig. 6 visualizes (4.2), and changed the problem to finding a plane α,

$$\alpha\left(\vec{F}^{\Delta_\phi}_{\Delta,l}\right) \geq 0 \quad \Longleftrightarrow \quad \sum_{\Delta,l} p_{\Delta,l} \vec{F}^{\Delta_\phi}_{\Delta,l} \neq 0 \ . \tag{4.3}$$

Our goal is to find out which scaling dimensions Δ and spins l are allowed with respect to OPE coefficients $f_{\phi\phi\mathcal{O}}$, so we can first make an assumption of Δ and l, then test if the crossing equation can be sovled or not. By keep trying different sets of Δ and l, we will find the boundary between allowed and disallowed region, which can tell us more physical information.

4.1 A Special Example

In this specific example [10], we are given a tailored linear functional α that is close enough to the boundary to show the physics behind the conformal bootstrap. $\vec{F}^{\Delta_\phi}_{\Delta,l}$ in the vector space takes the form,

$$\vec{F} = \left(H\left(\frac{1}{2},\frac{3}{5}\right) - H\left(\frac{1}{2},\frac{1}{3}\right), H\left(\frac{1}{2},\frac{3}{5}\right) - H\left(\frac{1}{3},\frac{1}{4}\right)\right) \tag{4.4}$$

$$H(z,\bar{z}) = \frac{F(u,v)}{u^{\Delta_\phi} - v^{\Delta_\phi}} \ ,$$

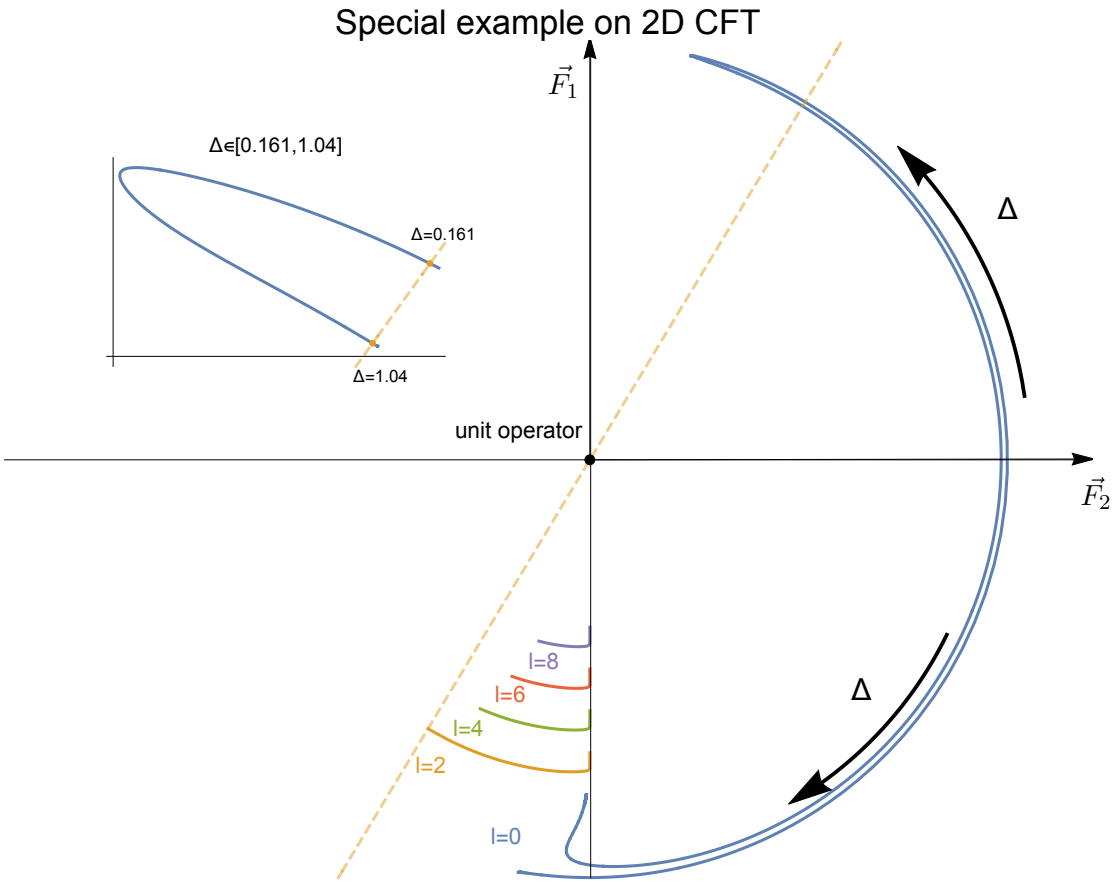

Figure 7: The two axes of the plot are the coordinates of the components of $\vec{F}$ in (4.4), which are labeled by $\vec{F}_1$ and $\vec{F}_2$ respectively. Each curve represents a $\vec{F}$ of a different spin l with respect to the scaling dimension Δ. Δ moves clockwise for most spins, but it moves in both direction for spin zero case. In order to show the difference between clockwise and counter-clockwise, we rescaled the normalized $\vec{F}$ for some decreasing functions. Despite of the rescale, the fact that all curves are converging to the vertical axis $\vec{F}_1$ is obvious.

where $F(u,v) \equiv \vec{F}^{\Delta_\phi}_{\Delta,l}$ is given by (4.2), and the conformal blocks in which are given by (3.12). We give the plot of normalized $\vec{F}$ with $\Delta_\phi = 1/8$ in Fig. 7.

Recall that the goal is to find the allowed and disallowed regions for Δ (from the subscript of $\vec{F}^{\Delta_\phi}_{\Delta,l}$) by finding the plane α. If the plane can be found, then the Δ cannot exist. We can also think of the procedure conversely. We first find a plane that contains most points of widest range (which is not easy for higher dimensions), then we see if there are any points outside this plane. If there are points that the plane can not cover, we know there exists Δ that solves the crossing equation (4.1). In our 2D example, the plane is the dashed line in Fig. 7. The dashed line connects the starting point for $l = 2$, which is the most distant point to the $\vec{F}_1$ axis, and the unit operator, which has to be strictly positive. So the interception of the dashed line α and blue curve $\vec{F}^{\frac{1}{8}}_{\Delta,0}$ gives the boundary of allowed and disallowed region for Δ. The epilog of Fig. 7 gives the more detailed plot around the boundary, and shows that only 2D CFT with $\Delta \in [0.161, 1.04]$ can exist. Indeed, the 2D Ising model with $\Delta = 1$ exists.

The example above was splendid, showing how the conformal bootstrap work by finding the

disallowed region. However, the splendid example was too rare, and one can hardly find an analytical way to show the boundary in higher dimensions. In fact, even finding a appropriate functional in (4.4) is very difficult, not to mention solving it. But things can be worked out numerically, and the disallowed region has a new name in numerical bootstrap, the dual-feasible.

4.2 Bootstrap

The numerical bootstrap has a complete, standard, easy-to-use procedure. The first part of it is still to find a functional α. The functional commonly used in numerical bootstrap is [10],

$$\alpha(F) = \sum_{m+n\leq\Lambda} a_{mn} \frac{\partial^m}{\partial z^m}\frac{\partial^n}{\partial \bar{z}^n} F(z,\bar{z})\Big|_{z=\bar{z}=\frac{1}{2}} \geq 0 \ , \tag{4.5}$$

where Λ is some integer called derivative cutoff, and a_{mn} are some coefficients without any constraint. In priciple, the cutoff Λ can be chosen arbitrarily, because it is part of the definition of our functional. Now, our problem of finding the plane α has been changed to finding coefficients a_{mn}. For a certain set of (Δ, l), one can ask the computer to find the coefficients a_{mn} that satisfies (4.5). If (4.5) can be satisfied, then this set of (Δ, l) is not allowed by any CFT.

For our 4-point function, we want to find the region where $\phi \times \phi$ can exist, which is called the allowed region. To achieve the goal we use (4.5) to find the region of Δ where $\phi \times \phi$ cannot exist for all spins, which is called the disallowed region. The maximum value of disallowed Δ is called Δ_0. Then we truncate both disallowed regions and the region that is not allowed by the unitarity bounds (1.34), the region left in the space is the allowed region. So the complete problem is,

$$\begin{aligned}
&\sum_{m+n\leq\Lambda} a_{mn}\partial^m\partial^n F(z,\bar{z})\Big|_{z=\bar{z}=\frac{1}{2}} \geq 0 \quad \text{for all } \Delta \geq \begin{cases} \Delta_0 & l=0 \\ l+d-2 & l>0 \end{cases}, \ l=0,2,4,... \\
&\sum_{m+n\leq\Lambda} a_{mn}\partial^m\partial^n F(z,\bar{z})\Big|_{z=\bar{z}=\frac{1}{2}} > 0 \quad \text{for } \Delta=0, \ l=0.
\end{aligned} \tag{4.6}$$

where the second line is for the sum over unit operator to be strictly positive.

4.3 SDPB

The most important part of solving a numerical bootstrap is to find the coefficients for (4.6), and here we introduce the Semi-Definite Programing for Bootstrap (SDPB).

SDPB takes the input of a set of polynomial matrices,

$$M_j^n(x) = \begin{pmatrix} P^n_{j,11}(x) & \dots & P^n_{j,1m_j}(x) \\ \vdots & \ddots & \vdots \\ P^n_{j,m_j1}(x) & \dots & P^n_{j,m_jm_j}(x) \end{pmatrix} , \tag{4.7}$$

where $1 \leq j \leq J$ and $0 \leq n \leq N$ are some labels for matrices, and m_j is the dimension of

matrices. Then SDPB will try to solve the following problem,

$$\begin{aligned} &\text{maximize } b_0 + b \cdot y \qquad \text{over } y \in \mathbb{R}^N \ , \\ &\text{s.t. } M_j^0 + \sum_{n=1}^{N} y_n M_j^n \succeq 0 \quad \text{for all } x \geq 0 \text{ and } 1 \leq j \leq J \ , \end{aligned} \tag{4.8}$$

where b_0 and b are some extra parameters called objects, and y is the core problem we are interested in. The SDPB so far is still a mathematical problem, we need to change our $\alpha(F)$ (4.5) into the input (4.7) for SDPB, and the conditions in (4.6) into the SDPB problem. Therefore, we make the following correspondence in Mathematica,

Variables in Bootstrap and in SDPB		
Bootstrap	SDPB	Physical meaning
$\partial^m \partial^n F(z,\bar{z})\Big\|_{z=\bar{z}=\frac{1}{2}}$	$M_j^n(x)$	Functional for $\vec{F}_{\Delta,l}^{\Delta_\phi}$
$l = 0, 2, 4, ...$	$j = 1, 2, 3, ..., J$	Spin
$0 \leq m + n \leq \Lambda$	$0 \leq n \leq N$	Cutoff for the derivative
$\Delta \geq \begin{cases} \Delta_0 & l = 0 \\ l + d - 2 & l > 0 \end{cases}$	$x \geq 0$	Assumption of Δ_0
unit operator	n	Normalization

We omitted the first line of the condition in (4.8) because there is no physical meaning in it. Although we want to test our assumption of Δ_0 for all spin l, we can not set the spin to infinity on a computer. So we have to compromise and set the maximum J to some large even number. At the last line of the table, there is one condition with physical meaning in (4.6) having no correspondence in SDPB, the unit operator. So we make use of a parameter call normalization in SDPB, and our problem becomes,

$$\begin{aligned} &\text{maximize } b \cdot y \qquad \text{over } y \in \mathbb{R}^N \ , \\ &\text{s.t. } \sum_{n=0}^{N} y_n M_j^n \geq 0 \quad \text{for all } x \geq 0 \text{ and } 1 \leq j \leq J \ , \\ &\qquad\qquad \text{with normalization } n \cdot y = 1 \ . \end{aligned} \tag{4.9}$$

Recall that we need the sum over unit operator to be strictly positive, and the coefficients y_n can be rescaled arbitrarily without breaking the non-negativity of the sum over M_j^n. So we set $n \cdot y = 1$ to satisfy the condition on the unit operator.

To conclude, the SDPB will tell you if y_n can be found for given M_j^n. We perform SDPB to every set of our assumption (Δ_ϕ, Δ_0), which is a point of our plot in the next section, to know whether the assumption should be included in the disallowed region or not.

4.4 The Ising Model

The Ising[3] model is used to describe critical points by lattice approximation. Consider a spin structure on a lattice model with spin-up $\uparrow$ and spin-down $\downarrow$, denoted by $s_i = \pm 1$. The partition

[3] German pronunciation: ˈiːzɪŋ

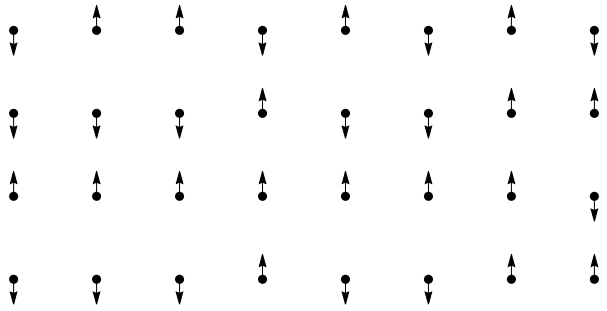

Figure 8: The 2D Ising model with random spins. Each s_i is a point with spin in the plot.

function is [16],

$$\mathcal{Z} = \sum_{s_i} e^{K \sum_{\langle ij \rangle} s_i s_j} \ , \tag{4.10}$$

where the subscript $\langle ij \rangle$ indicates s_j is the neighbourhood to s_i. K is the coupling constants. There is a $\mathbb{Z}_2$ symmetry under fliping all the spins at the same time because of the unchanging $\sum_{\langle ij \rangle} s_i s_j$.

Now consider a system with temperature $T = \frac{1}{K}$, and the coupling constant K goes to infinity when T is close to zero. At the low temperature limit, any configuration with negative $s_i s_j$ will not contribute, i.e. all lattices tend to have the same spin. If there is a fluctuation making a random s_i change its spin, the probability of making s_j change the spin is zero due to the partition function. So there is no correlation bewtween s_i and s_j. In high temperature limit, the coupling constants K goes to 0. So any $s_i s_j$ contribute the same, i.e. there is no correlation again.

But at finite non-zero temperature, the correlation exists due to the preference of the partition function. There is a critical point K_c where the correlation length is infinity. We can zoom out continously and find the conformal invariance at the critical point. The critical point K_c of the 2D Ising model is given in [1].

To study the field theory, we need to make a map between discreted lattices and continous fields. At long distance we have the approximation [10],

$$\begin{aligned} \mathbb{Z}^d &\longrightarrow \mathbb{R}^d \ , \\ s_i &\longrightarrow \phi(x) \ , \\ \sum_{s_i} &\longrightarrow \int \mathcal{D}\phi \ , \\ e^{K \sum_{\langle ij \rangle} s_i s_j} &\longrightarrow e^{S[\phi]} \ . \end{aligned} \tag{4.11}$$

The action of 3D Euclidean scalars is,

$$S[\phi] = \int d^3x \left(\frac{1}{2} (\partial \phi)^2 + \frac{1}{2} m^2 \phi^2 + g \phi^4 \right) \ , \tag{4.12}$$

the critical ratio $m^2/g^2 = r_c$ corresponds to the critical temperature K_c [16]. The $\mathbb{Z}_2$ symmetry corresponds to the odd local operator σ even local operator ϵ in CFT [17]. The 2D Ising model

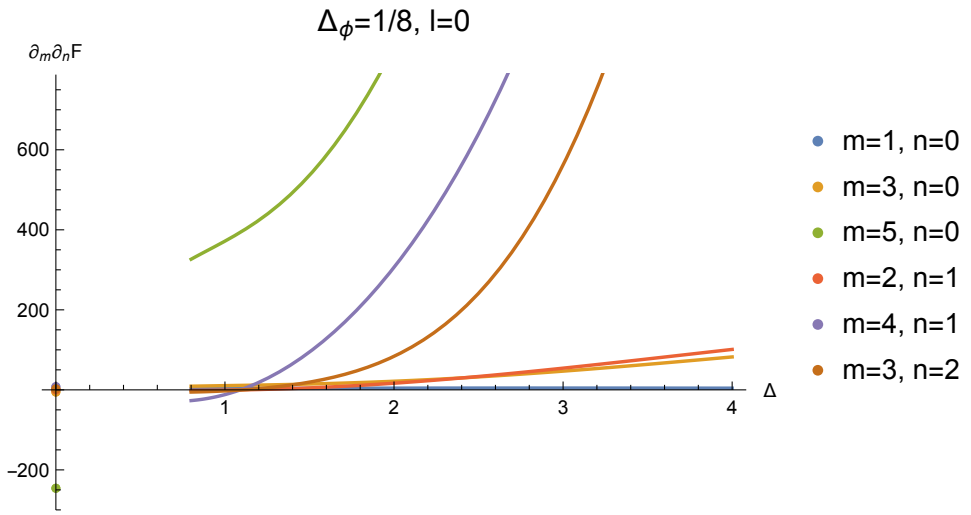

Figure 9: The result of $\partial^m\partial^n F(z,\bar{z})\Big|_{z=\bar{z}=\frac{1}{2}}$ with respect to Δ is based on the output of scalar_blocks. The points on the y-axis are the unit operators. We can simply take $\partial^4\partial^1 F(z,\bar{z})\Big|_{z=\bar{z}=\frac{1}{2}}$ to be our functional $\alpha(F)$, and ignore the unit operator (the vaccum can be excluded from the Hilbert space in some cases [22]),then we will find region below $\Delta_0 = 1.1$ is the allowed region. The result is only 10% away from the relation between Δ_σ and Δ_ϵ obtained via minimal model, and the error will almost vanish when using SDPB.

is solved by the minimal model with $(\Delta_\sigma, \Delta_\epsilon) = (1/8, 1)$. We will see the solution again in terms of the conformal bootstrap in the next chapter.

4.5 2D and 3D Bootstrap

We start with a famous example of the conformal bootstrap showing the existence of 2D Ising model, which is first accomplished in [18].

Our first step is to obtain the functional $\alpha(F)$ in (4.5), for which we need to compute the conformal blocks in $\vec{F}^{\Delta_\phi}_{\Delta,l}$ (4.2) and then compute the derivatives of it. Therefore we use the scalar_blocks [4], which generates the derivatives of the conformal block directly as a replacing list in Mathematica. After taking the derivatives of $\vec{F}^{\Delta_\phi}_{\Delta,l}$ without knowing the exact form of it, we replace the derivatives with the output of scalar_blocks (See Fig. 9).

The second step is to input the functional as a one-dimensional matrix into SDPB, and SDPB will tell you whether it is dual-feasible, which means the assumption is disallowed. There are two key inputs for SDPB, the unit operator as the normalization condition, and the functional $\alpha(F)$ with respect to Δ_0.

The first two steps can be view as a function of Δ_0. There are only two values for this function, the dual-feasible denoting the disallowed region, and primal-feasible denoting the the allowed region (after considering unitarity bounds). Since we want to know the boundary between the dual-feasible and the primal-feasible, we can perform binary search to bring our

[4]The code is based on Zamolodchikov-like recursion relations [19]. The higher-dimensional blocks in are discussed in [20, 8], and the even-dimensional blocks are discussed in [21].

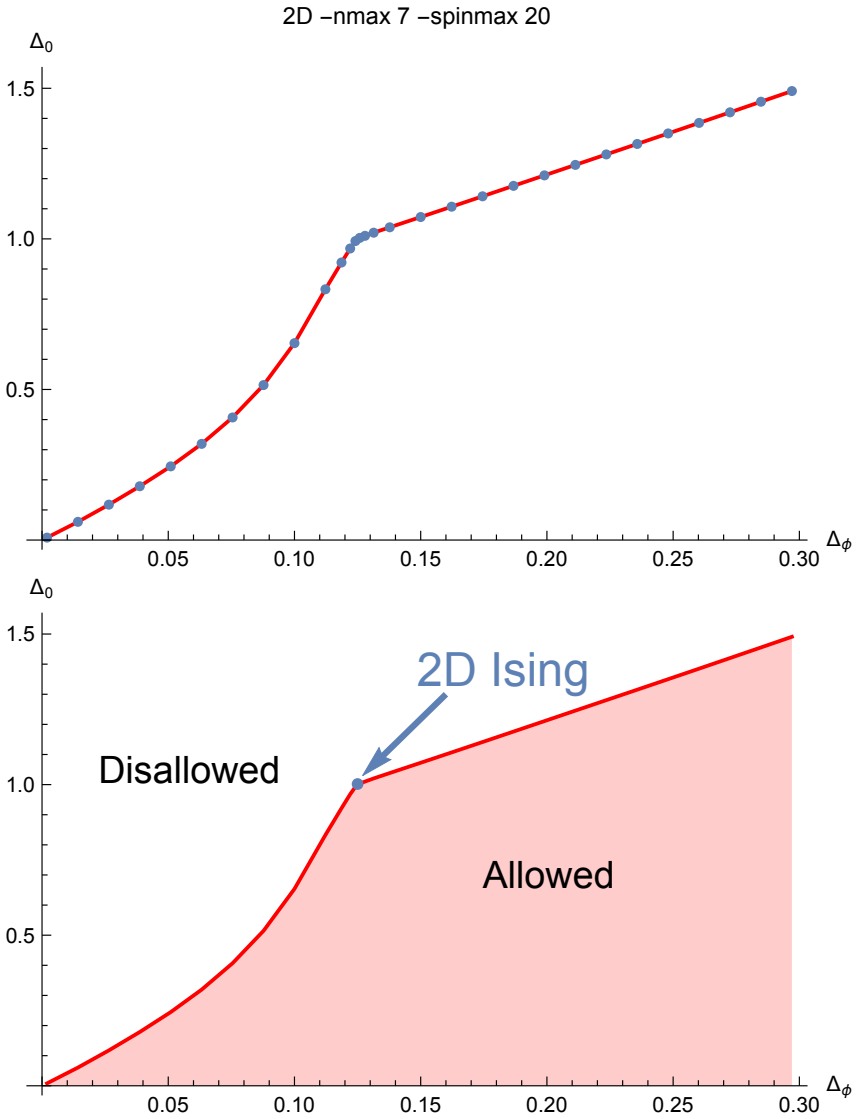

Figure 10: The plot shows the final output of our binary search. The region between the red curve and the Δ_ϕ axis is the allowed region.

boundary to any precision.

The upper plot of Fig. 10 shows the origin output of $\phi \times \phi$ OPE in 2D, where each point represents a boundary for given Δ_ϕ. We find a kink around $(1/8, 1.002)$, where the 2D Ising model exists with $\Delta = 1$, which is slightly below the disallowed region. It is a great evidence that the bootstrap doesn't exclude the 2D Ising model!

Apart from the two key inputs for SDPB, there are two parameters which are related to "how good the boundary is", -nmax $\equiv \lfloor \frac{\Lambda+1}{2} \rfloor$ and -spinmax $\equiv J$. As we mentioned before, we want to make J as big as possible because it should be at infinity in principle. And for the cutoff, the great the better.

We compared the boundary of different -spinmax and -nmax in Fig. 11 We can see that with higher -nmax, our boundary is getting squeezed towards the Δ_ϕ axis, which means more disallowed region has been excluded. Also, there is a converging behavior for the boundary with

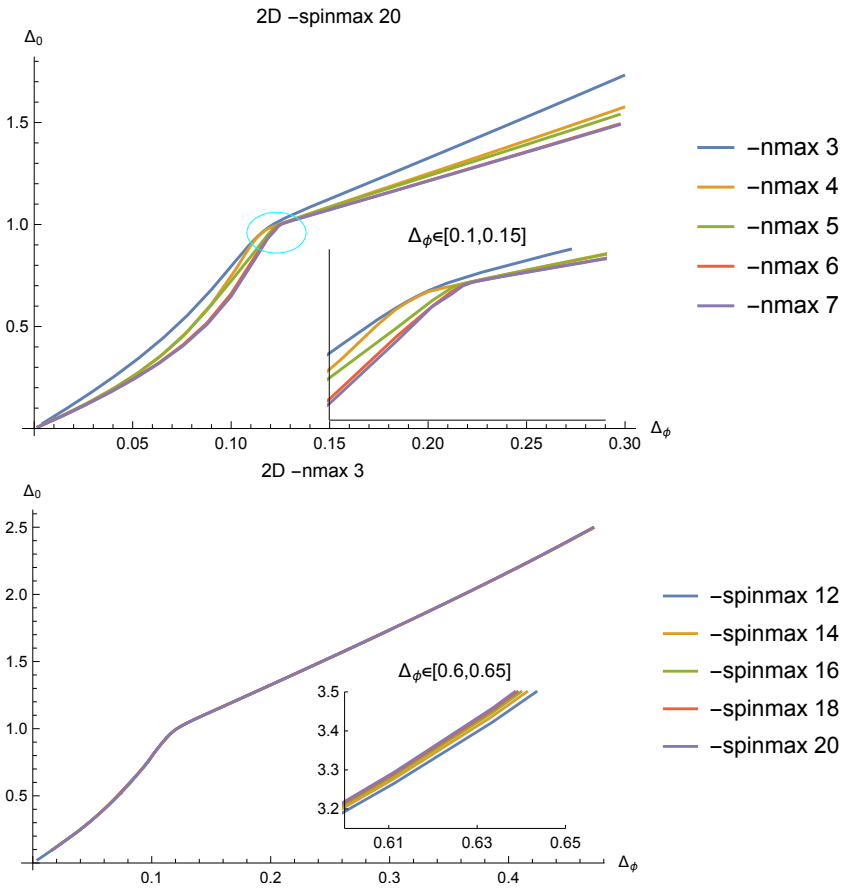

Figure 11: The plot shows how -nmax and -spinmax affect the boundary as parameters for the functional and the SDPB respectively. The inset small plots are the detailed plots for the parts circled in cyan.

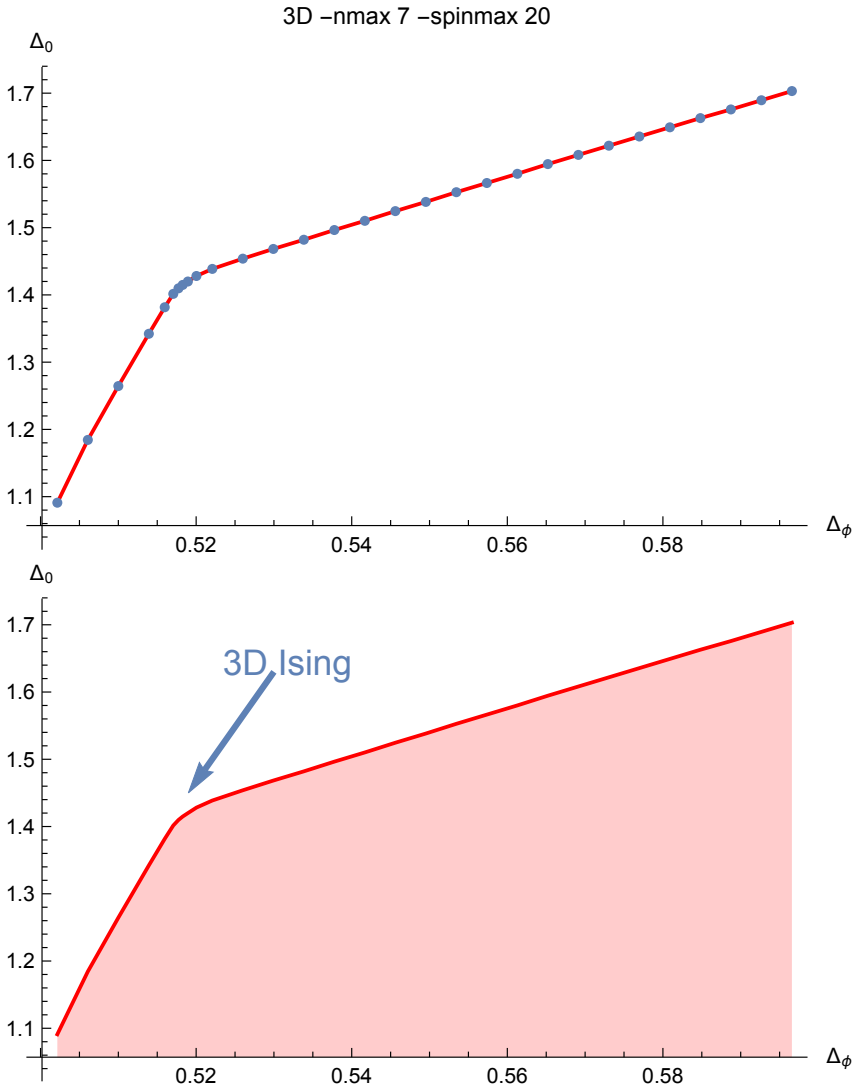

Figure 12: The final output for 3D bootstrap.

increasing -nmax. There is an obvious space bwtween -namx 3 and -nmax 4 (blue and yellow), but one can hardly see the difference when we go from -nmax 5 to -nmax 6 (red and purple). On the other hand, having -spinmax instead of infinity is a compromise. We cannot claim the region disallowed unless we have tried all spins, which is impossible on a computer. So we hope for the converging behavior for -spinmax as well. The difference between difference -spinmax is very little at small Δ_ϕ, but we can still see the subtle difference at large Δ_ϕ in the epilog of lower plot of Fig. 11.

The allowed region (between boundary and the Δ_ϕ axis) is decreasing with larger -nmax, and increasing with larger -spinmax. The intuitive explaination to this is: the higher the -nmax is, the more terms of derivatives we have in (4.6), the better chance to get the sum above zero, the more region to be truncated; the higher the -spinmax is, the more functionals in (4.6) we need to check, the less likely to find a set of coefficients satisfying (4.6) for all spins, the less region to be truncated. Ideally, we will have a converging true boundary with -namx ∞ -spinmax ∞, above which no CFT can exist. But numerically, we can claim our boundary is close enough

to the true boundary if no significant difference is found when we further increase -nmax and -spinmax.

We also computed the $\phi \times \phi$ OPE in 3D with -namx 7, and -spinmax 12 because we find the plot is stable when we further increase the parameters. The Δ_ϕ starts with 0.5 is because the unitarity boundary has excluded the region below $(d-2)/2$. The kink around $(0.518, 1.41)$ is believed to be where 3D Ising models exist, and one can further locate the scaling dimensions in a small island for 3D Ising models by doing bootstrap to different operators such as $\langle\sigma\sigma\epsilon\epsilon\rangle$ and $\langle\epsilon\epsilon\epsilon\epsilon\rangle$ [20].

5 Discussion

We have now grasped the basics of the numerical conformal bootstrap, and given the plot of 2D and 3D conformal bootstrap for four identical scalar fields. The 2D plot shows that the conformal bootstrap didn't exclude the existing theory, which makes the technique more persuasive. As for the 3D plot, it is a prediction for 3D Ising models that no exact solution has been found. Based on the result we obtained in 3D bootstrap, we can further consider correlators of mixing operators with different scaling dimensions. This will give a stronger prediction of the solution for 3D Ising models. In addition to Ising models, $O(N)$ can describe phase transition with higher degrees of freedom [8]. In the future, we will discover more physical meaning of Ising models such as phase transitions, and extend the degrees of freedom to $O(N)$ vector models.

Another task we can achieve in the conformal bootstrap topic is to make the program work more efficiently. There are options in the SDPB that we haven't introduced but related to finding the solution, by modifying which one can run the code with fewer iterations but higher precisions.

References

[1] L. Onsager,
Crystal statistics. 1. A Two-dimensional model with an order disorder transition, Phys. Rev. **65** (1944) 117–149.

[2] S. El-Showk, M. F. Paulos, D. Poland, S. Rychkov, D. Simmons-Duffin and A. Vichi,
Solving the 3D Ising Model with the Conformal Bootstrap, Phys. Rev. D **86** (2012) 025022, [1203.6064].

[3] S. El-Showk, M. F. Paulos, D. Poland, S. Rychkov, D. Simmons-Duffin and A. Vichi,
Solving the 3d Ising Model with the Conformal Bootstrap II. c-Minimization and Precise Critical Expone
J. Stat. Phys. **157** (2014) 869, [1403.4545].

[4] A. M. Polyakov, Conformal symmetry of critical fluctuations, JETP Lett. **12** (1970) 381–383.

[5] D. Poland and D. Simmons-Duffin, The conformal bootstrap, Nature Phys. **12** (2016) 535–539.

[6] A. A. Belavin, A. M. Polyakov and A. B. Zamolodchikov,
Infinite Conformal Symmetry in Two-Dimensional Quantum Field Theory, Nucl. Phys. B **241** (1984) 333–380.

[7] P. Di Francesco, P. Mathieu and D. Senechal, Conformal Field Theory. Graduate Texts in Contemporary Physics. Springer-Verlag, New York, 1997, 10.1007/978-1-4612-2256-9.

[8] F. Kos, D. Poland and D. Simmons-Duffin, Bootstrapping the $O(N)$ vector models, JHEP **06** (2014) 091, [1307.6856].

[9] M. Maggiore, A Modern introduction to quantum field theory. Oxford Master Series in Physics, 2005.

[10] D. Simmons-Duffin, The Conformal Bootstrap, in
Theoretical Advanced Study Institute in Elementary Particle Physics:
New Frontiers in Fields and Strings, pp. 1–74, 2017. 1602.07982. DOI.

[11] S. Rychkov, EPFL Lectures on Conformal Field Theory in D>= 3 Dimensions.
SpringerBriefs in Physics, 1, 2016, 10.1007/978-3-319-43626-5.

[12] M. Hogervorst, M. Paulos and A. Vichi, The ABC (in any D) of Logarithmic CFT, JHEP **10** (2017) 201, [1605.03959].

[13] M. Hogervorst and S. Rychkov, Radial Coordinates for Conformal Blocks, Phys. Rev. D **87** (2013) 106004, [1303.1111].

[14] M. S. Costa, J. Penedones, D. Poland and S. Rychkov, Spinning Conformal Blocks, JHEP **11** (2011) 154, [1109.6321].

[15] F. A. Dolan and H. Osborn, Conformal partial waves and the operator product expansion, Nucl. Phys. B **678** (2004) 491–507, [hep-th/0309180].

[16] D. Simmons-Duffin, Advanced Mathematical Methods: Conformal Field Theory , in Notes for Physics 229, 2017-2018, 2020.

[17] D. Poland, S. Rychkov and A. Vichi, The conformal bootstrap: Theory, numerical techniques, and applications, Rev. Mod. Phys. **91** (Jan, 2019) 015002.

[18] V. S. Rychkov and A. Vichi, Universal Constraints on Conformal Operator Dimensions, Phys. Rev. D **80** (2009) 045006, [0905.2211].

[19] P. K. Walter Landry, David Simmons-Duffin, My article, .

[20] F. Kos, D. Poland and D. Simmons-Duffin, Bootstrapping Mixed Correlators in the 3D Ising Model, JHEP **11** (2014) 109, [1406.4858].

[21] P. Kravchuk, Unpublished, .

[22] S. Collier, P. Kravchuk, Y.-H. Lin and X. Yin, Bootstrapping the Spectral Function: On the Uniqueness of Liouville and the Universality of BTZ, JHEP **09** (2018) 150, [1702.00423].